A fully nonlinear Boussinesq model for surface waves. Part 1. Highly nonlinear unsteady waves

By GE WEI[1], JAMES T. KIRBY[1], STEPHAN T. GRILLI[2], AND RAVISHANKAR SUBRAMANYA[2]

[1]Center for Applied Coastal Research, University of Delaware, Newark, DE 19716, USA

[2]Department of Ocean Engineering, University of Rhode Island, Narragansett, RI 02882, USA

Fully nonlinear extensions of Boussinesq equations are derived to simulate surface wave propagation in coastal regions. By using the velocity at a certain depth as a dependent variable (Nwogu 1993), the resulting equations have significantly improved linear dispersion properties in intermediate water depths when compared to standard Boussinesq approximations. Since no assumption of small nonlinearity is made, the equations can be applied to simulate strong wave interactions prior to wave breaking. A high-order numerical model based on the equations is developed and applied to the study of two canonical problems: solitary wave shoaling on slopes and undular bore propagation over a horizontal bed. Results of the Boussinesq model with and without strong nonlinearity are compared in detail to those of a boundary element solution of the fully nonlinear potential flow problem developed by Grilli *et al.* (1989). The fully nonlinear variant of the Boussinesq model is found to predict wave heights, phase speeds and particle kinematics more accurately than the standard approximation.

1. Introduction

Boussinesq-type equations, which include the lowest-order effects of nonlinearity and frequency dispersion as additions to the simplest non-dispersive linear long wave theory, provide a sound and increasingly well-tested basis for the simulation of wave propagation in coastal regions. The standard Boussinesq equations for variable water depth were first derived by Peregrine (1967), who used depth-averaged velocity as a dependent variable. Numerical models based on Peregrine's equations or equivalent formulations have been shown to give predictions which compare quite well with field data (Elgar & Guza 1985) and laboratory data (Goring 1978; Liu, Yoon & Kirby 1985; Rygg 1988), when applied within their range of validity.

Owing to the assumptions of weak dispersion and weak nonlinearity, the standard Boussinesq equations are restricted to shallow water areas and to small nonlinear effects. The first restriction results from the fact that the polynomial dispersion relation in standard Boussinesq equations mimics the exact linear solution (based on a hyperbolic tangent function) poorly in intermediate and deep water. Recently, extended forms of Boussinesq equations have been derived by Madsen, Murray & Sørensen (1991) and Nwogu (1993), among others. Madsen *et al.* achieved an improved linearized model by introducing expressions in the equations which are formally equivalent to zero within the accuracy of the model, thus obtaining a rearrangement of higher-order terms in the momentum equations. The form of the

added terms was governed by the constraint of obtaining the best possible linear dispersion relation. Nwogu (1993) used the velocity at a certain depth as a dependent variable and pursued a consistent derivation of the governing equations using this non-standard dependent variable. In the end, the choice of the representative depth was again constrained by the goal of obtaining the most accurate possible dispersion relation. Although the methods of derivation are different, the resulting dispersion relations of these extended Boussinesq equations are similar, and may be thought of as a slight modification of the (2,2) Padé approximant of the full dispersion relation (Witting 1984). Both expressions are much closer to the exact solution in intermediate water depths than are the standard Boussinesq equations. Madsen *et al.* and Nwogu have shown by example that the extended equations are able to simulate wave propagation from relatively deep to shallow water. Wei & Kirby (1995) developed a high-order numerical model based on Nwogu's equations, and provided additional validation tests of the model.

Despite their improved dispersion relation, the extended Boussinesq equations are still restricted to situations with weakly nonlinear interactions. In many practical cases, however, the effects of nonlinearity are too large to be treated as a weak perturbation to a primarily linear problem. As waves approach shore, wave height increases due to the effect of shoaling, and wave breaking occurs on most gentle natural slopes. The wave height to water depth ratios accompanying this physical process are inappropriate for weakly nonlinear Boussinesq models, and thus extensions to the model are required in order to obtain a computational tool which is locally valid in the vicinity of a steep, almost breaking or breaking wave crest.

An additional (and less obvious) limitation imposed by weak nonlinearity in the Boussinesq model occurs in the higher-frequency range, which is precisely the range of linear behaviour incorporated by the modifications of Madsen *et al.* and Nwogu. As an illustration, we consider the range of validity for Boussinesq wave models in figure 1, where the horizontal and vertical axes represent dispersive effects ($\mu^2 = (kh)^2$) and nonlinear effects ($\delta = a/h$), respectively. The standard Boussinesq equations are based on the assumption that $\delta, \mu \ll 1$ and $\delta/\mu^2 = O(1)$, after which terms of $O(\mu^4, \delta\mu^2, \delta^2)$ are neglected. The range of validity is thus bounded not only by some arbitrary value for δ and μ^2, but also by the curve c_1 which represents some value of $\delta\mu^2$. For the sake of illustration, let us suppose that the limit of validity for the standard approximation corresponds approximately to $\delta = \mu^2 = 0.2$. The value of c_1 is then around 0.04, as shown in figure 1. It is apparent that the limit of usefulness of the standard model is not controlled primarily by c_1, which represents the neglected nonlinear effects in dispersion terms. If we introduce the model extensions of Madsen *et al.* or Nwogu, however, the implied limit of validity for μ^2 becomes much higher. We see that this extended region is reduced in size by the neglected nonlinear dispersive terms, represented by the region above c_1.

The extension of the range of validity of the linear models achieved by Madsen *et al.* and Nwogu is limited in the nonlinear regime by the fact that the curve c_1 approaches the horizontal axis. This places serious constraints on the wave steepnesses which are actually allowed in intermediate water depth. The introduction of a fully nonlinear model within the context of the Boussinesq dispersion approximation formally pushes the upper envelope to a level controlled by the required smallness of $\delta\mu^4$, as illustrated by the curve c_2. We thus seek to achieve a wider range of validity for the model over the entire range of water depths.

Fully nonlinear models for moderately long water waves have been developed and studied for several decades. Using a power series expansion, Su & Gardner (1969)
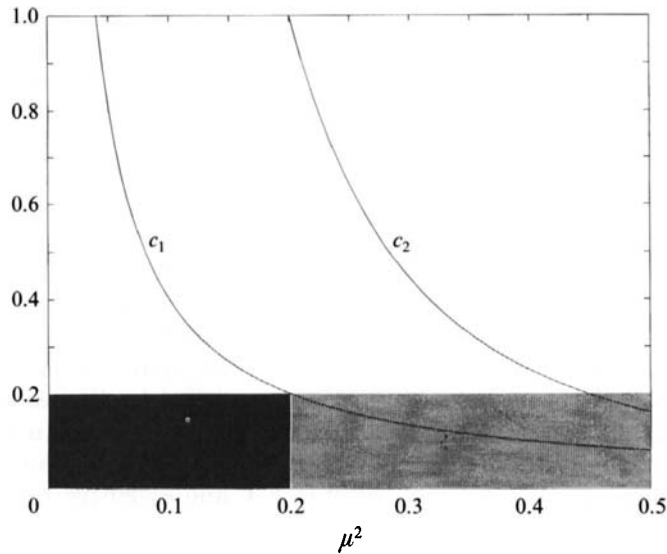
FIGURE 1. Hypothetical limits of validity of approximate long wave models. Dark gray - standard Boussinesq models. Light gray - additional region of validity for extended Boussinesq models of Madsen *et al.* (1991) and Nwogu (1993). Curve c_1 denotes $\delta\mu^2 = 0.04$. Curve c_2 denotes $\delta\mu^4 = 0.04$.

investigated a fully nonlinear formulation from which they were able to derive KdV and Burgers equations for a class of nonlinear Galilean-invariant systems. Using standard perturbation methods and the depth-averaged velocity, Mei (1989) derived Boussinesq equations for constant depth with no assumption of small nonlinearity. Neither of these models was utilized in any practical calculations.

The theory of fluid sheets proposed by Green & Naghdi (1976) provides an alternate method for constructing model equations for nonlinear wave propagation. In most applications of Green & Naghdi's method, a polynomial approximation of the internal flow field structure is introduced into the integral conservation laws. The resulting models approximately satisfy the field equations, but nonlinear free surface boundary conditions are exactly satisfied. Demirbilek & Webster (1992) have described an application of Green & Naghdi's method to the development of a shallow water wave model. Numerous computational examples were provided, but no comparison to experimental data or more exact solutions to the governing equations was made. Miles & Salmon (1985) obtained equations equivalent to Green & Naghdi's first level of approximation by employing Hamilton's variational principle. They further obtained a canonical form of Boussinesq equations, using the velocity potential at the still water level as the dependent variable. No computations were carried out, and, in fact, this model is formally unstable for large values of the wavenumber.

Perturbation methods and the theory of fluid sheets reduce the dimensionality of the original water wave problem by one, but the resulting equations are no longer exact. Alternatively, numerical schemes can be developed to directly solve the original fully nonlinear potential flow (FNPF) problem, for which there is no error in the governing equations. Following the principles outlined by Longuet-Higgins & Cokelet (1976) for the computations of two-dimensional space-periodic deep water waves, many investigators developed increasingly accurate and general FNPF models. The FNPF model of Grilli, Skourup & Svendsen (1989) and Grilli (1993) solves the

original equations in physical space, using a two-dimensional boundary element method (BEM) formulation that reduces dimensionality by one. This model has been extensively tested against laboratory data for the case of shoaling and breaking solitary waves by Grilli *et al.* (1994a). The results of this comparison show that the FNPF model predictions are in strikingly close agreement with measured data, and we thus accept the FNPF model as a standard of accuracy in the examples considered below.

In this study, a fully nonlinear Boussinesq model (FNBM) is derived following the approach of Nwogu (1993), using the velocity at a certain depth as a dependent variable. We deviate from the usual Boussinesq approximation by retaining full nonlinearity in the free surface boundary conditions. Results of computations with the FNBM are compared to results of numerical solutions of the FNPF equations obtained using the BEM model of Grilli *et al.* (1989), and to results of the extended Boussinesq model (BM) of Nwogu (1993), as modelled by Wei & Kirby (1995). A detailed derivation of the FNBM equations is presented in § 2. In § 3, a high-order predictor - corrector method is developed to solve these equations. The boundary element solution of the FNPF is reviewed in § 4, and extensive references are given for more detailed explanations. In § 5, numerical results from Boussinesq models with and without strong nonlinearity are compared in detail to BEM results for solitary wave shoaling on slopes and undular bore propagation. A summary of findings and conclusions is presented in § 6. Additional analysis of the model in the intermediate depth regime (employing a Stokes expansion) will be addressed in Kirby & Wei (1995).

2. Derivation of equations

We proceed, using standard techniques, to construct the fully nonlinear form of the governing equations based on a series solution for Laplace's equation in the fluid interior. Following Mei (1989), we use a reference wavenumber k_0 to scale horizontal distances x, y, a reference water depth h_0 to scale the vertical coordinate z and local depth $h(x, y)$ and amplitude a to scale the surface displacement η. We then introduce the parameters $\delta = a/h_0$ and $\mu^2 = (k_0 h_0)^2$. Based on these, we choose a scale of $(k_0(gh_0)^{1/2})^{-1}$ for time t and $\delta h_0(gh_0)^{1/2}/\mu$ for velocity potential ϕ. Introducing these scales into the boundary value problem for inviscid, irrotational motion leads to the problem

$$\phi_{zz} + \mu^2 \nabla^2 \phi = 0; \qquad -h \leqslant z \leqslant \delta\eta, \qquad (2.1)$$

$$\phi_z + \mu^2 \nabla h \cdot \nabla \phi = 0; \qquad z = -h, \qquad (2.2)$$

$$\eta + \phi_t + \tfrac{1}{2}\delta \left[(\nabla\phi)^2 + \frac{1}{\mu^2}(\phi_z)^2 \right] = 0; \qquad z = \delta\eta, \qquad (2.3)$$

$$\eta_t + \delta\nabla\phi \cdot \nabla\eta - \frac{1}{\mu^2}\phi_z = 0; \qquad z = \delta\eta. \qquad (2.4)$$

We develop an equation expressing volume flux conservation by integrating (2.1) over z from $-h$ to $\delta\eta$ and using (2.2) and (2.4) to obtain

$$\eta_t + \nabla \cdot M = 0; \qquad M = \int_{-h}^{\delta\eta} \nabla\phi \, \mathrm{d}z. \qquad (2.5)$$

In the following, we use (2.5) to obtain expressions for mass conservation, while a momentum equation is obtained using the Bernoulli equation (2.3). (This procedure is

not unique; for example, Mei (1989) proceeds by substituting approximate expressions for ϕ directly in the surface kinematic boundary condition rather than using an integrated volume conservation expression, while Nwogu (1993) and others use depth-integrated forms of the Euler equations to develop the momentum equations.)

2.1. *Approximate expression for the velocity potential*

As in previous studies of weakly dispersive shallow water waves, we reduce the dimensionality of the boundary value problem by introducing a series expansion for ϕ. An expression for ϕ which retains terms to $O(\mu^2)$ and satisfies the bottom boundary condition is given by

$$\phi = \phi_0(x,t) - \mu^2(h+z)\nabla h \cdot \nabla\phi_0 - \mu^2\frac{(h+z)^2}{2}\nabla^2\phi_0 + O(\mu^4) \tag{2.6}$$

where ϕ_0 is the value of the velocity potential at $z = -h$. In practice, we may replace ϕ_0 by the value of the potential at any level in the water column. Any choice will lead to a set of model equations with the same level of asymptotic approximation but with numerically different dispersion properties. Following Nwogu (1993) and Chen & Liu (1995), we denote ϕ_α as the value of ϕ at $z = z_\alpha(x, y)$, or

$$\phi_\alpha = \phi_0 - \mu^2(h+z_\alpha)\nabla h \cdot \nabla\phi_0 - \mu^2\frac{(h+z_\alpha)^2}{2}\nabla^2\phi_0 + O(\mu^4). \tag{2.7}$$

This expression is then used in (2.6) to obtain an expression for ϕ in terms of ϕ_α:

$$\phi = \phi_\alpha + \mu^2(z_\alpha - z)\nabla \cdot (h\nabla\phi_\alpha) + \tfrac{1}{2}\mu^2(z_\alpha^2 - z^2)\nabla^2\phi_\alpha + O(\mu^4). \tag{2.8}$$

This form of the velocity potential is then used in the governing equations to obtain the approximate models.

2.2. *Two-equation model for η and ϕ_α*

First, a two-equation model for η and ϕ_α is developed. The expression for M in (2.5) becomes

$$\begin{aligned}
M = (h + \delta\eta)&\left[\nabla\phi_\alpha + \mu^2\left\{\nabla\left[z_\alpha\nabla \cdot (h\nabla\phi_\alpha) + \tfrac{1}{2}z_\alpha^2\nabla^2\phi_\alpha\right]\right.\right.\\
&\left.\left.+\frac{(h-\delta\eta)}{2}\nabla(\nabla \cdot (h\nabla\phi_\alpha)) - \frac{(h^2 - h\delta\eta + (\delta\eta)^2)}{6}\nabla^2\nabla\phi_\alpha\right\}\right].
\end{aligned} \tag{2.9}$$

The expression goes to zero identically as the total depth $h + \delta\eta$ goes to zero, which serves as a natural shoreline boundary condition.

The corresponding form of the Bernoulli equation (2.3) becomes

$$\begin{aligned}
&\eta + \phi_{\alpha t} + \tfrac{\delta}{2}(\nabla\phi_\alpha)^2 + \mu^2\left[(z_\alpha - \delta\eta)\nabla \cdot (h\nabla\phi_{\alpha t}) + \tfrac{1}{2}(z_\alpha^2 - (\delta\eta)^2)\nabla^2\phi_{\alpha t}\right]\\
&\quad + \delta\mu^2\left\{\nabla\phi_\alpha \cdot [\nabla z_\alpha\nabla \cdot (h\nabla\phi_\alpha) + (z_\alpha - \delta\eta)\nabla(\nabla \cdot (h\nabla\phi_\alpha))]\right\}\\
&\quad + \delta\mu^2\left\{\nabla\phi_\alpha \cdot [z_\alpha\nabla z_\alpha\nabla^2\phi_\alpha + \tfrac{1}{2}(z_\alpha^2 - (\delta\eta)^2)\nabla(\nabla^2\phi_\alpha)]\right\}\\
&\quad + \delta\mu^2\left\{\tfrac{1}{2}[\nabla \cdot (h\nabla\phi_\alpha)]^2 + \delta\eta\nabla \cdot (h\nabla\phi_\alpha)\nabla^2\phi_\alpha + \tfrac{1}{2}(\delta\eta)^2(\nabla^2\phi_\alpha)^2\right\} = 0
\end{aligned} \tag{2.10}$$

Equations at the order of approximation of the usual Boussinesq theory may be immediately obtained by neglecting terms of $O(\delta)$ or higher in the $O(\mu^2)$ dispersive terms. The modified expression for volume flux M is

$$\begin{aligned}
M = (h + \delta\eta)\nabla\phi_\alpha + \mu^2&\left\{h\nabla\left[z_\alpha\nabla \cdot (h\nabla\phi_\alpha) + \tfrac{1}{2}z_\alpha^2\nabla^2\phi_\alpha\right]\right.\\
&\left.+\tfrac{1}{2}h^2\nabla(\nabla \cdot (h\nabla\phi_\alpha)) - \tfrac{1}{6}h^3\nabla^2\nabla\phi_\alpha\right\}
\end{aligned} \tag{2.11}$$

and the Bernoulli equation reduces to

$$\eta + \phi_{\alpha t} + \tfrac{1}{2}\delta(\nabla\phi_\alpha)^2 + \mu^2\left[z_\alpha\nabla\cdot(h\nabla\phi_{\alpha t}) + \tfrac{1}{2}z_\alpha^2\nabla^2\phi_{\alpha t}\right] = 0. \tag{2.12}$$

Equations (2.11) and (2.12) were given previously by Chen & Liu (1995). These results may be compared to the two-equation model of Wu (1981), which uses the depth-averaged value of ϕ. The models are the same to within rearrangements of dispersive terms.

2.3. *Three-equation model based on η and u_α*

We further introduce a horizontal velocity u_α as $u_\alpha = \nabla\phi|_{z_\alpha}$. Retaining terms to $O(\mu^2)$ and to all orders in δ gives a fully nonlinear version of the model with volume flux

$$M = (h + \delta\eta)\left[u_\alpha + \mu^2\left\{\left[\tfrac{1}{2}z_\alpha^2 - \tfrac{1}{6}(h^2 - h\delta\eta + (\delta\eta)^2)\right]\nabla(\nabla\cdot u_\alpha)\right.\right.$$
$$\left.\left. + \left[z_\alpha + \tfrac{1}{2}(h - \delta\eta)\right]\nabla(\nabla\cdot(hu_\alpha))\right\}\right] + O(\mu^4) \tag{2.13}$$

and momentum equation

$$u_{\alpha t} + \delta(u_\alpha\cdot\nabla)u_\alpha + \nabla\eta + \mu^2 V_1 + \delta\mu^2 V_2 = O(\mu^4) \tag{2.14}$$

where

$$V_1 = \tfrac{1}{2}z_\alpha^2\nabla(\nabla\cdot u_{\alpha t}) + z_\alpha\nabla(\nabla\cdot(hu_{\alpha t})) - \nabla\left[\tfrac{1}{2}(\delta\eta)^2\nabla\cdot u_{\alpha t} + \delta\eta\nabla\cdot(hu_{\alpha t})\right] \tag{2.15}$$

$$V_2 = \nabla\left[(z_\alpha - \delta\eta)(u_\alpha\cdot\nabla)(\nabla\cdot(hu_\alpha)) + \tfrac{1}{2}(z_\alpha^2 - (\delta\eta)^2)(u_\alpha\cdot\nabla)(\nabla\cdot u_\alpha)\right]$$
$$+ \tfrac{1}{2}\nabla\left[(\nabla\cdot(hu_\alpha) + \delta\eta\nabla\cdot u_\alpha)^2\right]. \tag{2.16}$$

The Boussinesq approximation of Nwogu (1993) is recovered by neglecting terms of $O(\mu^4, \delta\mu^2)$, yielding the expressions

$$M = (h + \delta\eta)u_\alpha + \mu^2\left\{\left(\tfrac{1}{2}hz_\alpha^2 - \tfrac{1}{6}h^3\right)\nabla(\nabla\cdot u_\alpha) + \left(hz_\alpha + \tfrac{1}{2}h^2\right)\nabla(\nabla\cdot(hu_\alpha))\right\} \tag{2.17}$$

and

$$u_{\alpha t} + \delta(u_\alpha\cdot\nabla)u_\alpha + \nabla\eta + \mu^2\left\{\tfrac{1}{2}z_\alpha^2\nabla(\nabla\cdot u_{\alpha t}) + z_\alpha\nabla[\nabla\cdot(hu_{\alpha t})]\right\} = O(\delta\mu^2, \mu^4) \tag{2.18}$$

As a final note, we point out that the fully nonlinear models derived here all have mass flux $M \to 0$ at the shoreline, where $h + \delta\eta \to 0$. This result is expected on physical grounds and appears in the nonlinear shallow water equations and in Boussinesq models where the depth-averaged velocity is the dependent variable. This condition is not automatically satisfied by Nwogu's or any weakly nonlinear Boussinesq model based on a velocity other than the depth-averaged value, making the application of these models problematic at the shoreline. All fully nonlinear variations of any of the possible model systems should recover this condition correctly.

3. Numerical scheme

A high-order predictor-corrector scheme is utilized to obtain the results described below. The scheme is similar to that of Wei & Kirby (1995), with the inclusion of extra nonlinear terms. The high-order numerical scheme is employed in order to eliminate truncation errors which have the same form as dispersive terms in the equations. Although the truncation terms will be eliminated in the limit as $\Delta x \to 0$, $\Delta y \to 0$, $\Delta t \to 0$ in any consistent schemes, these terms may be the same magnitude as dispersive terms for a second-order scheme using typical grid resolutions. Usually, back substitution of the truncation terms must be performed to

obtain accurate answers (Abbott, McCowan & Warren 1984; Nwogu 1993). In this study, we discretize the first-order spatial derivative terms to fourth-order accuracy by using standard five-point finite-differencing, leading to truncation errors of $O(\Delta x^4/\mu^2)$ relative to the dispersive terms. In contrast, the dispersive terms themselves are finite-differenced only to second-order accuracy, leading to error terms of $O(\Delta x^2)$ relative to the actual dispersive terms. The system of equations is written in a form that makes the application of a higher-order time-stepping procedure convenient. The fourth-order Adams–Bashforth–Moulton predictor-corrector scheme is employed to perform this updating. The high-order discretization of first-order spatial and temporal derivative terms guarantees that the truncation error terms do not have the same form as that of dispersive terms in the equations, and thus no back substitution is required.

The FNBM in dimensional form for two-dimensional flow can be rewritten as

$$\eta_t = E(\eta, u, v) + E_2(\eta, u, v), \tag{3.1}$$

$$[U(u)]_t = F(\eta, u, v) + [F_1(v)]_t + F_2(\eta, u, v, u_t, v_t), \tag{3.2}$$

$$[V(v)]_t = G(\eta, u, v) + [G_1(u)]_t + G_2(\eta, u, v, u_t, v_t), \tag{3.3}$$

where η is the surface elevation, u and v are the horizontal velocities at $z = z_\alpha = -0.531h$, and U and V are defined as

$$U = u + [b_1 h u_{xx} + b_2 (hu)_{xx}], \tag{3.4}$$

$$V = v + \left[b_1 h v_{yy} + b_2 (hv)_{yy}\right], \tag{3.5}$$

which are treated as simple variables in the time-stepping scheme. The remaining quantities E, E_2, F, F_1, F_2, G, G_1 and G_2 are spatial derivatives of η, u, v, u_t or v_t which are defined as

$$
\begin{aligned}
E = &-[(h+\eta)u]_x - [(h+\eta)v]_y \\
&- \left\{a_1 h^3 (u_{xx} + v_{xy}) + a_2 h^2 [(hu)_{xx} + (hv)_{xy}]\right\}_x \\
&- \left\{a_1 h^3 (u_{xy} + v_{yy}) + a_2 h^2 [(hu)_{xy} + (hv)_{yy}]\right\}_y,
\end{aligned}
\tag{3.6}
$$

$$F = -g\eta_x - (uu_x + vu_y), \tag{3.7}$$

$$G = -g\eta_y - (uv_x + vv_y), \tag{3.8}$$

$$F_1 = -h\left[b_1 h v_{xy} + b_2 (hv)_{xy}\right], \tag{3.9}$$

$$G_1 = -h\left[b_1 h u_{xy} + b_2 (hu)_{xy}\right], \tag{3.10}$$

$$
\begin{aligned}
E_2 = &- \left\{\left[a_1 h^2 \eta + \tfrac{1}{6}\eta(h^2 - \eta^2)\right](u_{xx} + v_{xy})\right\}_x \\
&- \left\{\left[a_2 h\eta - \tfrac{1}{2}\eta(h+\eta)\right][(hu)_{xx} + (hv)_{xy}]\right\}_x \\
&- \left\{\left[a_1 h^2 \eta + \tfrac{1}{6}\eta(h^2 - \eta^2)\right](u_{xy} + v_{yy})\right\}_y \\
&- \left\{\left[a_2 h\eta - \tfrac{1}{2}\eta(h+\eta)\right][(hu)_{xy} + (hv)_{yy}]\right\}_y,
\end{aligned}
\tag{3.11}
$$

$$
\begin{aligned}
F_2 = &- \left\{\tfrac{1}{2}(z_\alpha{}^2 - \eta^2)[u(u_x + v_y)_x + v(u_x + v_y)_y]\right\}_x \\
&- \left\{(z_\alpha - \eta)\left[u[(hu)_x + (hv)_y]_x + v[(hu)_x + (hv)_y]_y\right]\right\}_x \\
&- \tfrac{1}{2}\left\{[(hu)_x + (hv)_y + \eta(u_x + v_y)]^2\right\}_x \\
&+ \left\{\tfrac{1}{2}\eta^2[(u_t)_x + (v_t)_y] + \eta[h(u_t)]_x + [h(v_t)]_y\right\}_x,
\end{aligned}
\tag{3.12}
$$

$$G_2 = - \left\{ \tfrac{1}{2}(z_\alpha{}^2 - \eta^2)[u(u_x + v_y)_x + v(u_x + v_y)_y] \right\}_y$$

$$- \left\{ (z_\alpha - \eta) \left[u[(hu)_x + (hv)_y]_x + v[(hu)_x + (hv)_y]_y \right] \right\}_y$$

$$- \tfrac{1}{2} \left\{ [(hu)_x + (hv)_y + \eta(u_x + v_y)]^2 \right\}_y$$

$$+ \left\{ \tfrac{1}{2}\eta^2[(u_t)_x + (v_t)_y] + \eta([h(u_t)]_x + [h(v_t)]_y) \right\}_y. \tag{3.13}$$

E_2, F_2 and G_2 are the additional high-order nonlinear terms which would not exist for weakly nonlinear equations. The constants a_1, a_2, b_1, b_2 are defined as

$$a_1 = \beta^2/2 - 1/6, \quad a_2 = \beta + 1/2, \quad b_1 = \beta^2/2, \quad b_2 = \beta, \tag{3.14}$$

where $\beta = z_\alpha/h$. For the form of the Boussinesq equations based on depth-averaged velocity, the constants reduce to

$$a_1 = 0, \quad a_2 = 0, \quad b_1 = 1/6, \quad b_2 = -1/2. \tag{3.15}$$

The arrangement of cross-differentiated and nonlinear time-derivative terms on the right-hand side of equations (3.2)–(3.3) makes the resulting set of left-handed sides purely tridiagonal. The governing equations are finite-differenced on an un-staggered grid in $x = i\Delta x, y = j\Delta y, t = n\Delta t$. Level n refers to information at the present, known time level. The predictor step is the third-order explicit Adams–Bashforth scheme, given by

$$\eta_{i,j}^{n+1} = \eta_{i,j}^n + \frac{\Delta t}{12} \left[23(E')_{i,j}^n - 16(E')_{i,j}^{n-1} + 5(E')_{i,j}^{n-2} \right], \tag{3.16}$$

$$U_{i,j}^{n+1} = U_{i,j}^n + \frac{\Delta t}{12} \left[23(F')_{i,j}^n - 16(F')_{i,j}^{n-1} + 5(F')_{i,j}^{n-2} \right], \tag{3.17}$$

$$V_{i,j}^{n+1} = V_{i,j}^n + \frac{\Delta t}{12} \left[23(G')_{i,j}^n - 16(G')_{i,j}^{n-1} + 5(G')_{i,j}^{n-2} \right], \tag{3.18}$$

where

$$E' = E + E_2, \tag{3.19}$$

$$F' = F + (F_1)_t + F_2, \tag{3.20}$$

$$G' = G + (G_1)_t + G_2. \tag{3.21}$$

All information on the right-hand sides of (3.16)–(3.18) is known from previous calculations. The values of $\eta_{i,j}^{n+1}$ are thus straightforward to obtain. The evaluation of horizontal velocities at the new time level, however, requires simultaneous solution of tridiagonal matrix systems which are linear in the unknowns at level $n+1$. Specifically, for a given j, $u_{i,j}^{n+1}(i = 1, 2, ..., M)$ are obtained through tridiagonal matrix solution. Similarly, $v_{i,j}^{n+1}(j = 1, 2, ..., N)$ are solved by a system of tridiagonal matrix equation for given i. The matrices involved are constant in time and may be pre-factored, inverted and stored for use at each time step.

After the predicted values of $\eta_{i,j}^{n+1}$, $u_{i,j}^{n+1}$ and $v_{i,j}^{n+1}$ are evaluated, we obtain the corresponding quantities of $E_{i,j}^{n+1}$, $(E_2)_{i,j}^{n+1}$, $F_{i,j}^{n+1}$, $(F_2)_{i,j}^{n+1}$, $(F_2)_{i,j}^{n}$, $(F_2)_{i,j}^{n-1}$, $(F_2)_{i,j}^{n-2}$, $G_{i,j}^{n+1}$, $(G_2)_{i,j}^{n+1}$, $(G_2)_{i,j}^{n}$, $(G_2)_{i,j}^{n-1}$ and $(G_2)_{i,j}^{n-2}$, and apply the fourth-order Adams–Moulton corrector method

$$\eta_{i,j}^{n+1} = \eta_{i,j}^n + \frac{\Delta t}{24} \left[9(E')_{i,j}^{n+1} + 19(E')_{i,j}^n - 5(E')_{i,j}^{n-1} + (E')_{i,j}^{n-2} \right], \tag{3.22}$$

$$U_{i,j}^{n+1} = U_{i,j}^n + \frac{\Delta t}{24} \left[9(F')_{i,j}^{n+1} + 19(F')_{i,j}^n - 5(F')_{i,j}^{n-1} + (F')_{i,j}^{n-2} \right], \tag{3.23}$$

$$V_{i,j}^{n+1} = V_{i,j}^n + \frac{\Delta t}{24} \left[9(G')_{i,j}^{n+1} + 19(G')_{i,j}^n - 5(G')_{i,j}^{n-1} + (G')_{i,j}^{n-2}\right]. \tag{3.24}$$

From the definition, we see that the calculation of F_2 and G_2 at a certain time level requires the corresponding values of u_t and v_t. Also, the terms $(F_1)_t$ and $(G_1)_t$ involve time derivatives. For the predictor stage, values of u, v, F_1 and G_1 at the time level $n-2$, $n-1$ and n are known, then the corresponding derivatives are evaluated as

$$(w_t)_{i,j}^n = \frac{1}{2\Delta t} \left[3w_{i,j}^n - 4w_{i,j}^{n-1} + w_{i,j}^{n-2}\right] + O(\Delta t^2), \tag{3.25}$$

$$(w_t)_{i,j}^{n-1} = \frac{1}{2\Delta t} \left[w_{i,j}^n - w_{i,j}^{n-2}\right] + O(\Delta t^2), \tag{3.26}$$

$$(w_t)_{i,j}^{n-2} = \frac{-1}{2\Delta t} \left[3w_{i,j}^{n-2} - 4w_{i,j}^{n-1} + w_{i,j}^n\right] + O(\Delta t^2). \tag{3.27}$$

For the corrector stage, we evaluate w_t according to

$$(w_t)_{i,j}^{n+1} = \frac{1}{6\Delta t} \left[11w_{i,j}^{n+1} - 18w_{i,j}^n + 9w_{i,j}^{n-1} - 2w_{i,j}^{n-2}\right] + O(\Delta t^3). \tag{3.28}$$

$$(w_t)_{i,j}^n = \frac{1}{6\Delta t} \left[2w_{i,j}^{n+1} + 3w_{i,j}^n - 6w_{i,j}^{n-1} + w_{i,j}^{n-2}\right] + O(\Delta t^3), \tag{3.29}$$

$$(w_t)_{i,j}^{n-1} = \frac{-1}{6\Delta t} \left[2w_{i,j}^{n-2} + 3w_{i,j}^{n-1} - 6w_{i,j}^n + w_{i,j}^{n+1}\right] + O(\Delta t^3), \tag{3.30}$$

$$(w_t)_{i,j}^{n-2} = \frac{-1}{6\Delta t} \left[11w_{i,j}^{n-2} - 18w_{i,j}^{n-1} + 9w_{i,j}^n - 2w_{i,j}^{n+1}\right] + O(\Delta t^3), \tag{3.31}$$

where w represents u, v, F_1 or G_1 . The corrector step is iterated until the error between two successive results reaches a required limit. The error is computed for each of the three dependent variables η, u and v and is defined as

$$\Delta f = \frac{\sum_{i,j} |f_{i,j}^{n+1} - f_{i,j}^{(n+1)*}|}{\sum_{i,j} |f_{i,j}^{n+1}|} \tag{3.32}$$

where f denotes any of the variables and $()^*$ denotes the previous results. The corrector step is iterated if any of the Δf exceeds 10^{-4}.

For the weakly nonlinear case, the scheme typically requires no iteration unless problems arise from the boundary. However, for strong nonlinearity, the model tends to take more iterations. Further analysis showed that the iterated results oscillated around the desired solution. To increase the convergence rate, we applied an over-relaxation technique to the iteration stage. Writing the previous and current iterated values as $f_{i,j}^*$ and $f_{i,j}$, then the adjusted value $f_{i,j}^r$ for over-relaxation is given by

$$f_{i,j}^r = (1 - R)f_{i,j}^* + Rf_{i,j} \tag{3.33}$$

where R is a coefficient which is in the range $(0,1)$. In all computations, we found that $R = 0.2$ gave quite satisfactory results.

4. A review of the boundary element model

Equations and numerical methods for the FNPF model are briefly reviewed here. Details can be found in Grilli *et al.* (1989), Grilli (1993), and Grilli & Subramanya (1994). The velocity potential $\phi(x,t)$ is used to represent inviscid irrotational two-dimensional flows in the vertical plane (x,z) and the velocity is defined by $u = \nabla\phi =$
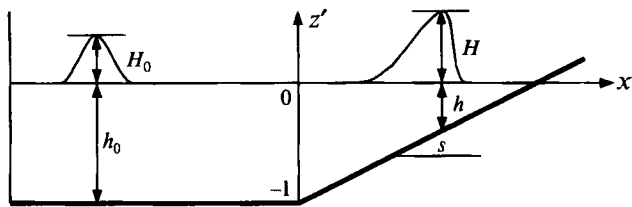
FIGURE 2. Definition sketch for both the FNPF computations and for the Boussinesq models.

(u, w) (figure 2). The continuity equation in the fluid domain $\Omega(t)$ with boundary $\Gamma(t)$ is Laplace's equation for the potential

$$\nabla^2 \phi = 0 \quad \text{in } \Omega(t). \tag{4.1}$$

Using the free space Green's function, $G(x, x_l) = -(1/2\pi) \log | x - x_l |$, and Green's second identity, equation (4.1) transforms into the boundary integral equation (BIE)

$$\alpha(x_l)\phi(x_l) = \int_{\Gamma(x)} \left[\frac{\partial \phi}{\partial n}(x)G(x, x_l) - \phi(x)\frac{\partial G(x, x_l)}{\partial n} \right] \, \mathrm{d}\Gamma(x) \tag{4.2}$$

in which $x = (x, z)$ and $x_l = (x_l, z_l)$ are position vectors for points on the boundary, n is the unit outward normal vector, and $\alpha(x_l)$ is a geometric coefficient.

Equation (4.2) is solved by a boundary element method (BEM), using a set of collocation nodes on the boundary and higher-order elements to interpolate in between the collocation nodes. Integrals in (4.2) are evaluated numerically and the resulting algebraic system of equations is assembled and solved for the equivalent discretized problem.

Along the stationary bottom Γ_b, a no-flow condition is prescribed by

$$\frac{\overline{\partial \phi}}{\partial n} = 0 \quad \text{on } \Gamma_b. \tag{4.3}$$

Waves can be generated in the model by simulating a piston wavemaker motion on the 'open sea' boundary of the computational domain, $\Gamma_{r1}(t)$, or by specifying the potential, ϕ, normal velocity, $\partial \phi / \partial n$, and the elevation, η, at initial time t_0 for the incident wave, directly on the free surface.

On the free surface $\Gamma_f(t)$, ϕ satisfies the kinematic and dynamic boundary conditions,

$$\frac{\mathrm{D}r}{\mathrm{D}t} = \left(\frac{\partial}{\partial t} + u \cdot \nabla \right) r = u = \nabla \phi \quad \text{on } \Gamma_f(t), \tag{4.4}$$

$$\frac{\mathrm{D}\phi}{\mathrm{D}t} = -gz + \tfrac{1}{2}\nabla \phi \cdot \nabla \phi - \frac{p_a}{\rho} \quad \text{on } \Gamma_f(t), \tag{4.5}$$

respectively, with r, the position vector on the free surface, g the gravitational acceleration, z the vertical coordinate, p_a the pressure at the free surface, assumed zero in the applications, and ρ the fluid density.

Free surface boundary conditions (4.4) and (4.5) are integrated in time based on two second-order Taylor series expansions for ϕ and r expressed in terms of a time step Δt and of the Lagrangian time derivative, $\mathrm{D}/\mathrm{D}t$, in a mixed Eulerian–Lagrangian formulation. Terms in both series expansions are calculated by solving two BIEs of the type (4.2) for ϕ and $\partial \phi / \partial t$ in sequence at each time step, the solution of the first BIE providing boundary conditions for the second BIE.

Trajectories of individual free surface particles – identical to nodes of the BEM discretization – are thus calculated as a function of time using the Taylor series. The time step in the model is adaptively selected based on a mesh Courant number to ensure optimal accuracy and stability of the computations (optimal value ≈ 0.5). In the applications, spatial and temporal discretizations were selected for the errors on wave volume and energy to stay to within 0.05% during most of the wave propagation (see Grilli & Subramanya 1994, for details of typical discretizations, numerical parameters, and computational errors for solitary wave shoaling in shallow water).

5. Results

The fully nonlinear Boussinesq model (FNBM) and the FNPF model described above were applied to study two cases of one-dimensional wave propagation. By setting $E_2 = F_2 = G_2 = 0$ in the FNBM, we also recover Nwogu's modified Boussinesq model (BM), in which nonlinearity is assumed to be small but dispersive properties are improved compared to standard Boussinesq models. Results from the extended Boussinesq models with and without strong nonlinearity are compared in detail with FNPF results for the examples shown below. In the first casestudy, computations of solitary waves shoaling over plane slopes are made. We consider three solitary waves with different initial height, $\delta = H_0/h_0$, propagating over four different slopes s ranging from gentle (1:100) to steep (1:8) (figure 2). We compare the wave shapes, shoaling rates, crest celerity and other properties for the three models. The second case involves undular bores of initial height H_0 propagating into water of constant depth h_0, with a nonlinearity parameter $\delta = H_0/h_0$. The shapes and heights of the bores are compared for three initial conditions corresponding to weak and strong nonlinearity. As expected, for cases with strong nonlinearity, results from the FNBM compare much better with the FNPF results than those of the BM, due to the additional nonlinear terms included in FNBM.

5.1. *Solitary wave shoaling on slopes*

The first example considered is the shoaling of solitary waves over a plane slope. The solitary wave example is a good test for the model in that it allows for a careful test of the propagation speed of an isolated pulse in the absence of any extra noise sources (such as reflections). In addition, the wave height to water depth ratios reached prior to breaking are higher than for most periodic incident waves, and thus a more severe test is made of the nonlinear portion of the model.

Figure 2 shows the computational domain, which consists of a constant depth h_0 on the left and a constant slope s on the right. Coordinates were set such that the toe of the slope correspond to $x = 0$. In the Boussinesq models, solitary waves were generated at the leftward boundary and propagated to the right. Four different slopes of $s = 1:100$, 1:35, 1:15 and 1:8 are used in the computations. On each slope, the incident wave height is varied from $\delta = 0.2$ to $\delta = 0.6$, which corresponds to a variation from weak to strong nonlinearity in the incident wave. The length, time and velocity variables are scaled by h_0, $(h_0/g)^{1/2}$ and $(gh_0)^{1/2}$, respectively, and the resulting dimensionless variables are denoted by primes.

The permanent-form solitary wave solution obtained for the same initial height in the three models is different due to different levels of approximation in the equations. In the FNPF computations, an exact solution of the fully nonlinear equations, obtained using Tanaka's (1986) method, was used as an initial wave and introduced
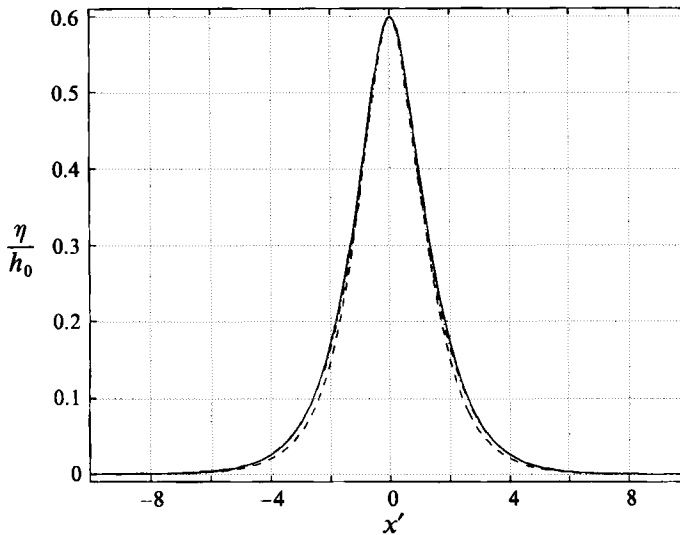
FIGURE 3. Comparison of FNPF (———), BM (- - - - -), and FNBM (— · —) for incident solitary wave shape for $\delta = 0.6$.

directly on the free surface. Wei & Kirby (1995) derived an approximate analytical solution to the BM equations assuming weak nonlinearity. In order to obtain initial conditions for the present computations, we first ran the BM and FNBM models with the approximate expression for the solitary wave as initial condition. This solution was run over a long distance with constant depth. At the beginning of these computations, wave heights and wave shapes kept changing, and small oscillatory tails developed behind the main waves as they propagated in the models. After running the models for a long time, however, the changes of form became negligible and wave shapes stabilized, indicating that a numerical permanent-form solitary wave solution corresponding to each of the Boussinesq models was obtained. These solutions were then used as input for the computations of solitary wave shoaling over slopes. Since the initial wave changed shape and height in the BM and FNBM model runs, several runs were required to obtain a permanent-form solitary wave with the desired height. A comparison of the incident solitary wave for the three models for the most nonlinear wave height $\delta = 0.6$ is shown in figure 3. The shape for the BM solitary wave is narrower than for the Tanaka solution. In contrast, the solitary wave shape produced by the FNBM solution is almost indistinguishable from the Tanaka solution, with discrepancies limited to a slight narrowing of the crest seen at elevations around half the wave height above the still water level. To account for the slight difference in solitary wave solutions for constant depth in the three models, results of computations were synchronized at $t' = 0$ in the comparison when wave crests reached the toe of the slope, $x' = 0$.

A comparison of evolving solitary wave profiles obtained in the three models is shown in figure 4. The four plots, (a), (b), (c) and (d) correspond to slopes of 1:100, 1:35, 1:15, and 1:8, respectively. The wave heights are $\delta = 0.2$ for (a), (b) and (d) but $\delta = 0.3$ for (c). The first profile to the left in each figure corresponds to the waves being at a location roughly half way up the slope. Wave asymmetry is not too pronounced yet, and one can see that both Boussinesq solutions agree quite well with the FNPF solution. The last profile in figure 4(a, b, c) corresponds to the
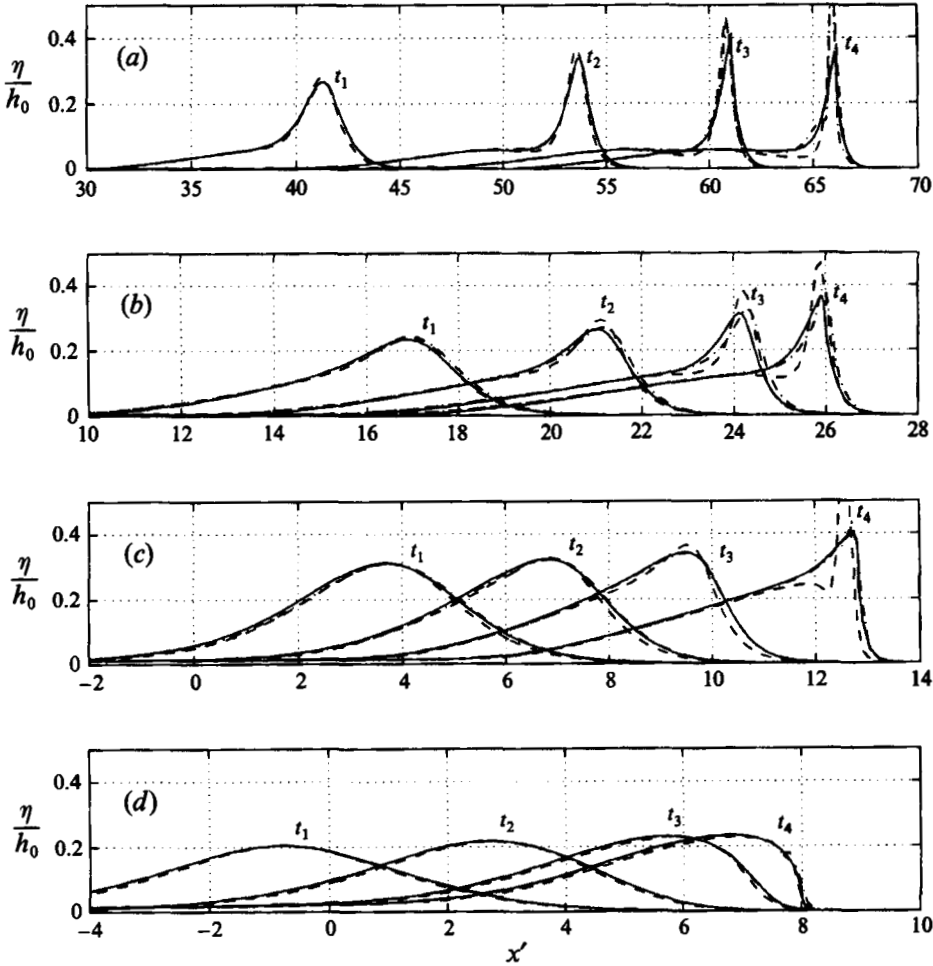
FIGURE 4. Comparison between FNPF (———), BM (- - - - -), and FNBM (— · —) of free surface elevations for the shoaling of solitary waves, with $\delta = 0.2$ in (a), (b), and (d) and 0.3 in (c). (a) $s = 1:100$; $t' = t_1 = 39.982$, $t_2 = 53.191$, $t_3 = 61.131$, $t_4 = 66.890$; (b) $s = 1:35$; $t' = t_1 = 16.243$, $t_2 = 20.640$, $t_3 = 24.032$, $t_4 = 25.936$; (c) $s = 1:15$; $t' = t_1 = 3.230, t_2 = 6.000$, $t_3 = 8.401$, $t_4 = 11.320$; (d) $s = 1:8$; $t' = t_1 = -0.739$, $t_2 = 2.575$, $t_3 = 5.576 = t_4 = 6.833$. The last FNPF profile in (a)–(c) corresponds to the theoretical breaking point for which the wave front face has a vertical tangent.

theoretical breaking points in the FNPF computations, for which the wave has a vertical tangent on the front face. No breaking occurs for the condition in figure 4(d). Breaking occurs in figure 4(b) for $t' = 25.94$ at $x'_b = 25.90$, and with a breaking index $H_b/h_b = 1.402$. This breaking point was found by Grilli *et al.* (1994a, b) to also closely correspond to measured breaking locations and characteristics in well-controlled laboratory experiments.

Results in figure 4 show that, with both the BM and the FNBM models, the wave crests travel almost at the right speed in the early shoaling. For the $s = 1:100$ slope, the BM and FNBM wave crests continue to grow in height while the FNPF pitches forward and decreases in height just prior to breaking. The results of the FNPF and FNBM models differ most in this case. For the steeper beaches the FNBM predicts

both the wave height and crest position with much greater accuracy than the BM model. The BM results on the three mildest slopes indicate that the wave significantly overshoals as compared to the FNPF results, particularly in the upper slope region, and a spurious secondary trough is predicted behind the main crest. With the FNBM, however, overshoaling is much less pronounced, and the spurious troughs are almost non-existent.

Results for the relative wave height, H/h, computed with all three models, are given in figure 5 as a function of x'. Symbols ($\circ$) denote the FNPF breaking point, determined by the x' location where the wave reaches a vertical tangent on the front face. One can see that, as expected from the above discussion, relative wave height is significantly overpredicted at the breaking point in the BM, whereas little or no overprediction occurs in the FNBM. Beyond the theoretical breaking point, wave heights grow in an unbounded fashion in both Boussinesq models. Figure 5 also shows that, with the BM, overshoaling mostly occurs in the region of high nonlinearity (i.e. high H/h) closer to the breaking point. This is due to insufficient nonlinear effects included in the BM equations; much of the error is eliminated in the FNBM.

Wave celerities were calculated for three incident wave heights, for each slope, using all three models. First, we obtained the time series of the crest location x'_c. Then three-point finite differencing was applied to compute the crest celerity c'_c. The estimation of the celerity values from the Boussinesq models was fairly straightforward, and the results are well represented by an 11-point running average fit to the values of c'_c. For the FNPF model, the celerity estimates exhibited a great deal of jitter, and also exhibited a much more complex functional dependence on x' due to the rapid change of the wave crest at and just beyond the breaking point. For this model, results are presented in terms of a 25th-order polynomial fit to the original raw data. All data processing was done using Matlab.

Results are reported in figure 6 for the crest celerity $c'_c = (\mathrm{d}x_c/\mathrm{d}t)(gh_0)^{1/2}$, as a function of crest location x'_c. The corresponding incident wave celerity c'_0 is almost identical in all three models. Results show that both Boussinesq models slightly underpredict the wave crest celerity as compared to the FNPF results for most of the shoaling process, with a larger discrepancy close to the breaking point. This was already observed in figure 4.

Particle velocity at the crest is defined as $V'_c = (u'^2_c + w'^2_c)^{1/2}$, where u'_c and w'_c are the horizontal and vertical velocity components. The comparison of V'_c for all three models is shown in figure 7(a, b, d) for $\delta = 0.2$ and in figure 7(c) for $\delta = 0.3$, where corresponding crest celerities have also been reproduced from figure 6. The FNPF model predicts, as expected, that $V'_c \geqslant c'_c$ at breaking on the three milder slopes (in fact slightly beyond the breaking point). The particle velocity at the crest in the BM starts diverging from the FNPF solution about half way up the slope and becomes quite large. This result is due to the overshoaling in the BM wave and the resulting overprediction of downward crest curvature. In contrast, the particle velocity in the FNBM stays quite close to the FNPF prediction up to the breaking point for all but the gentlest slopes. In fact, despite the discrepancies at breaking in the FNBM, $V'_c = c'_c$ (i.e. breaking) occurs at roughly the same location as in the FNPF model.

Vertical profiles of horizontal velocity at three different locations are shown in figure 8 for the case of 1:35 slope and wave height $\delta = 0.2$. In the Boussinesq models, the horizontal velocity at a certain depth $z = z_\alpha = -0.531h$ and the corresponding derivatives are computed. Then the variation of horizontal and vertical velocity with
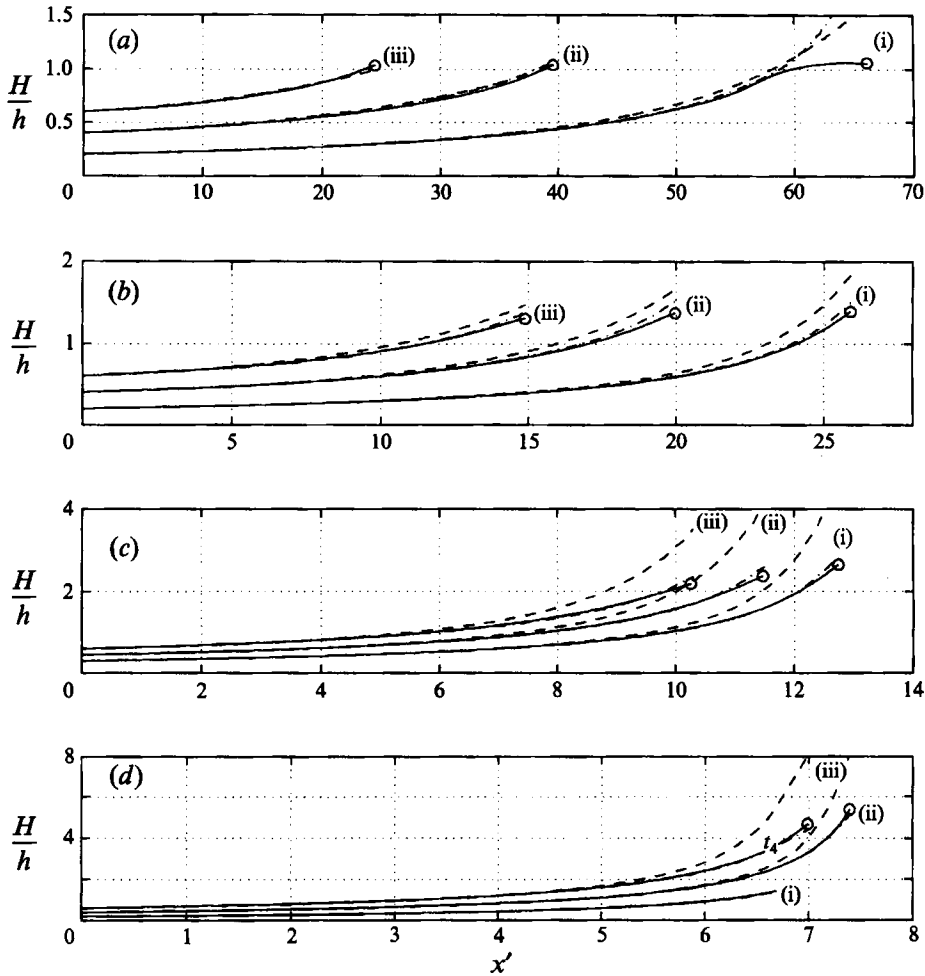
FIGURE 5. Comparison between FNPF (——), BM (- - - - -), and FNBM (— - —) of shoaling rates, H/h, for solitary waves with δ = (i) 0.20, (ii) 0.40, (iii) 0.60 in $(a),(b),(d)$ and δ = (i) 0.30, (ii) 0.45, (iii) 0.60 in (c); shoaling on a slope: (a) 1:100; (b) 1:35; (c) 1:15; (d) 1:8. Symbols (o) denote locations of the breaking point for which the wave has a vertical tangent on the front face.

water depth z is given by

$$u = u_\alpha + \frac{z_\alpha^2 - z^2}{2}(u_\alpha)_{xx} + (z_\alpha - z)(hu_\alpha)_{xx},$$ (5.1)

$$w = -(h + z)(u_\alpha)_x - h_x u_\alpha.$$ (5.2)

Generally, the velocity profiles of FNBM compare quite well with those of FNPF. The FNBM predict average, surface and bottom velocities reasonably accurately, the main discrepancy being the underprediction of profile curvature owing to the limitation of the quadratic velocity profile used in the model formulation. Most notably, the prediction of the kinematics retains its accuracy up to the wave breakpoint.

The comparison of velocity profiles between BM and FNPF is less satisfactory. The combined effects of incorrectly predicted values of u_α and the overprediction of wave heights and crest curvature in the BM result in larger horizontal velocities, especially
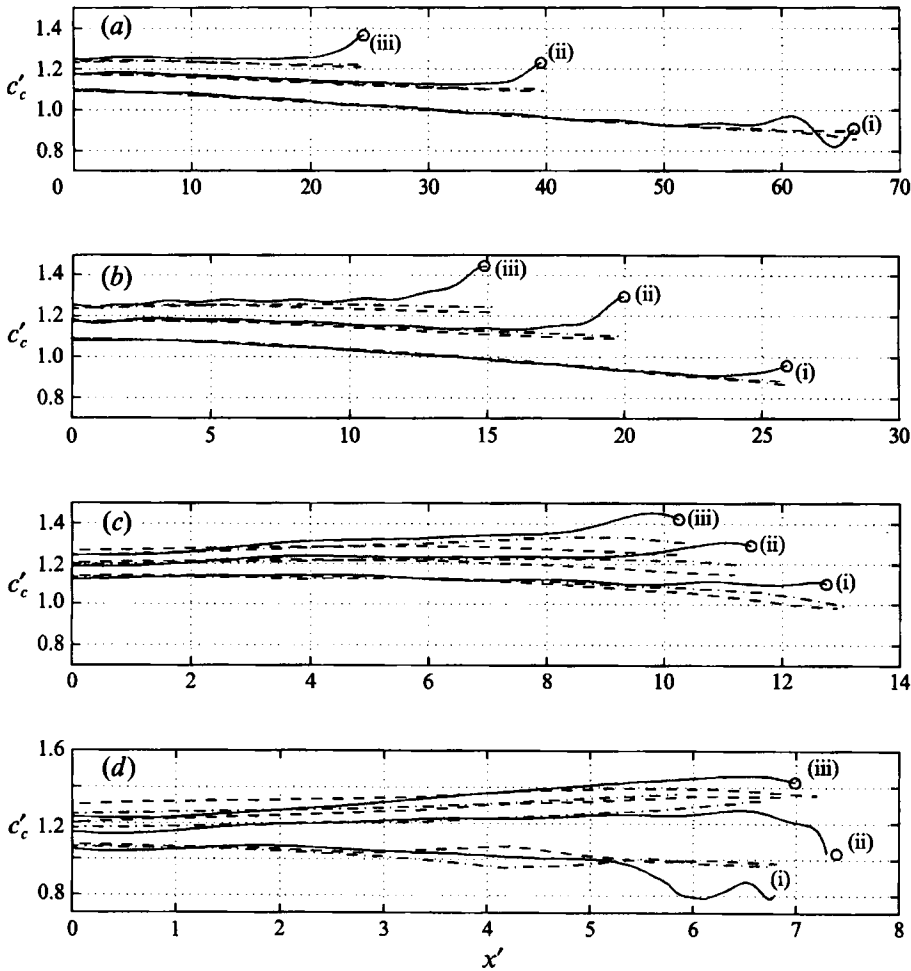
FIGURE 6. Comparison between FNPF (——), BM (- - - - -), and FNBM (— - —) of crest celerity c_c' for the same solitary waves and slopes as in figure 5. Symbols (○) are defined as in figure 5.

at the crest. Horizontal velocities are overpredicted by almost 50% over much of the final stage of shoaling in the BM.

5.2. Evolution of an undular bore

The second example chosen to compare the three models is that of an undular bore propagating into constant-depth, still water. This problem has been studied by a number of investigators and serves as a standard illustration of competing effects of dispersion and nonlinearity. Peregrine (1966) compared the differences between Boussinesq theory and Airy's theory for nonlinear long waves using this example. As shown in figure 9, the initial condition is a gentle transition between a uniform flow and still water:

$$u = \tfrac{1}{2}u_0[1 - \tanh(x/a)], \tag{5.3}$$

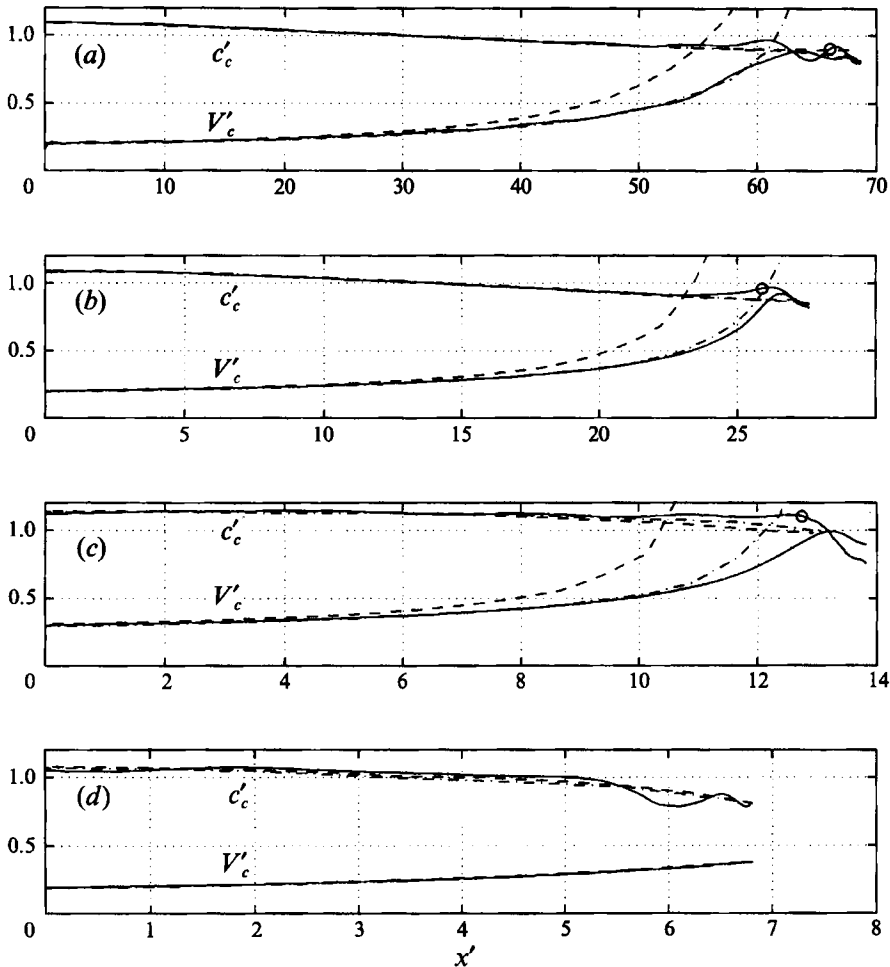$$\eta = u + \tfrac{1}{4}u^2, \tag{5.4}$$

FIGURE 7. Comparison between FNPF (———), BM (- - - - -), and FNBM (— - —) of wave crest celerity c'_c and particle velocity at the crest (components (u'_c, w'_c); value V'_c), for the same solitary waves and slopes as in figure 4. Symbols (o) are defined as in figure 5.

where η and u are the surface elevation and the horizontal velocity, x is the horizontal coordinate with $x = 0$ corresponding to the centre of the initial bore, u_0 is the velocity of uniform flow from the left boundary, and a is a number sufficiently large enough that the initial motion could be described by Airy's theory. In all the computation below, we use $a = 5$. Three different values of u_0 are chosen so that the surface elevations at the left boundary are $\eta_0 = 0.1, 0.2, 0.3$. Owing to the presence of vertical acceleration in the transition region between the two uniform-depth asymptotes, waves are generated from the initial smooth transition in models incorporating dispersive effects. The number and height of waves increases gradually with time, until a nearly uniform cnoidal wave train is developed which radiates the energy lost in the transition from one uniform depth to another.

In order to compute the initial evolution of the undular bore, the initial solution $(\eta(x), u(x))$ used in Peregrine (1966) is introduced as the initial wave. For the FNPF
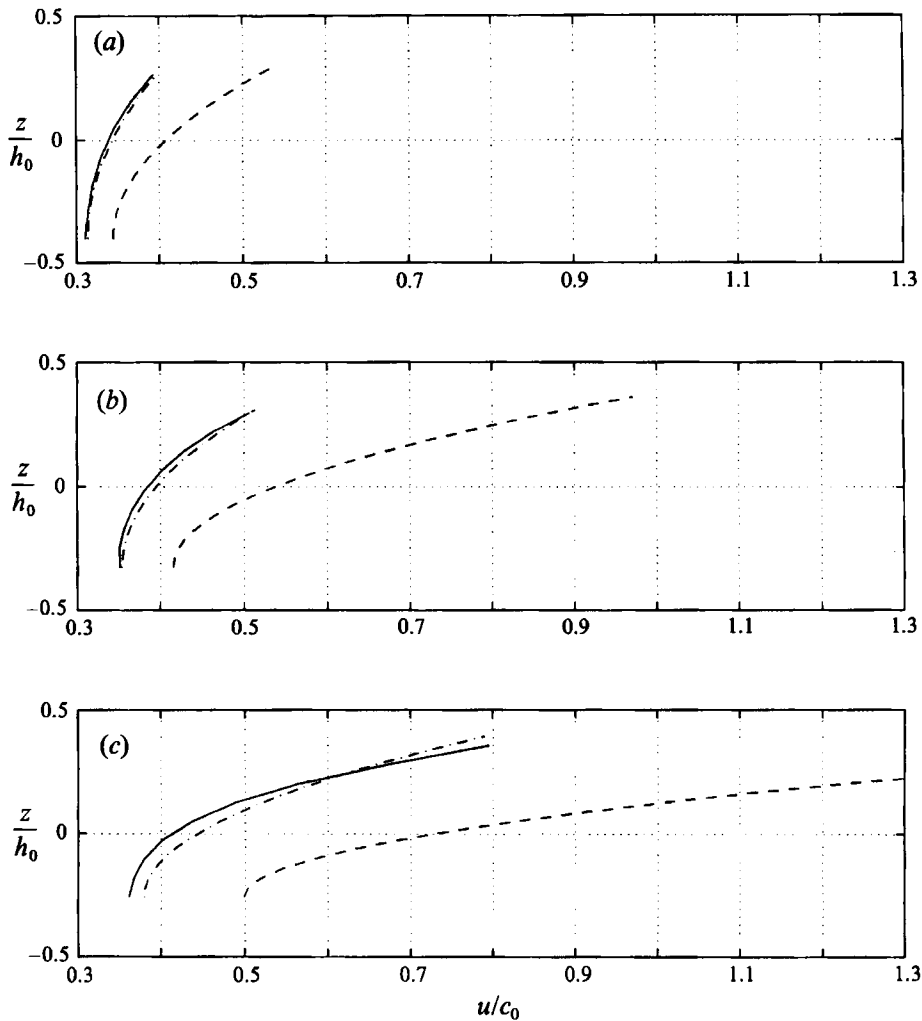
FIGURE 8. Comparison between FNPF (———), BM (- - - - -), and FNBM (— - —) of horizontal velocity profiles with initial height $\delta = 0.2$ on slope 1:35 at different locations: (a) $x' = 20.96$; (b) $x' = 23.63$; (c) $x' = 25.91$.

model, the corresponding initial free surface potential $\phi(x)$ is obtained by integrating $u(x)$ as a function of x and the initial normal velocity $\partial \phi / \partial n(x)$ is obtained by projecting $u(x)$ on the normal direction.

Figures 9 and 10 show the comparison of wave profiles at different times. For small values of η_0 as in plot (a), results from BM and FNBM are very close, indicating that the effects of the higher-order nonlinear terms in FNBM are negligible for small nonlinearity. For large values of η_0 as in (b) and (c), the wave heights predicted by BM are larger than those predicted by FNBM, and the predictions of the FNBM agree more closely with the FNPF model. In addition, the wave crest speeds predicted by FNBM are closer to FNPF model results than are those predicted by BM for all wave crests in the evolving wave train.

In figure 11, we plot the elevations of the first three wave crests and wave troughs
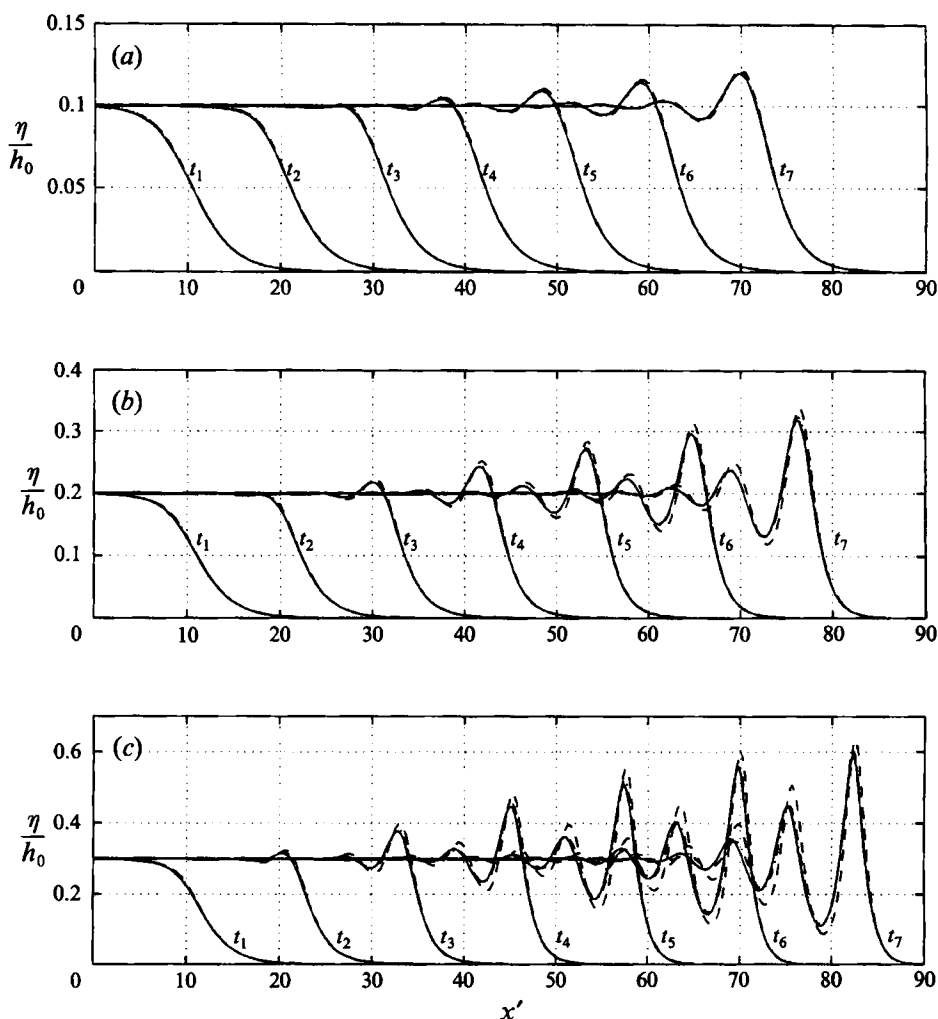
FIGURE 9. Comparison between FNPF (———), BM (- - - - -), and FNBM (—-—-—) of free surface elevations for undular bores with initial height δ = (a) 0.10; (b) 0.20; and (c) 0.30 at times t': $t_1 = 10$, $t_2 = 20$, $t_3 = 30$, $t_4 = 40$, $t_5 = 50$, $t_6 = 60$, $t_7 = 70$.

as a function of distance travelled for the same three conditions as in figures 9 and 10. We see that, in general, both crest elevations and trough depths increase with time, as was noted by Peregrine and other investigators. For small nonlinearity (figure 11a), results from BM are similar to those of FNBM, and both Boussinesq models overpredict wave height compared to the FNPF model. However, for large nonlinearity, the FNBM does a reasonable job of predicting the height of the leading wave crest and an excellent job of predicting the subsequent crests and troughs, compared to the FNPF. The wave heights from BM are no longer close to those of FNBM, indicating that the additional nonlinear terms in FNBM are important for this case. Aside from the phase speed difference, the wave crests and troughs from FNBM compare quite well with the predictions of the FNPF.
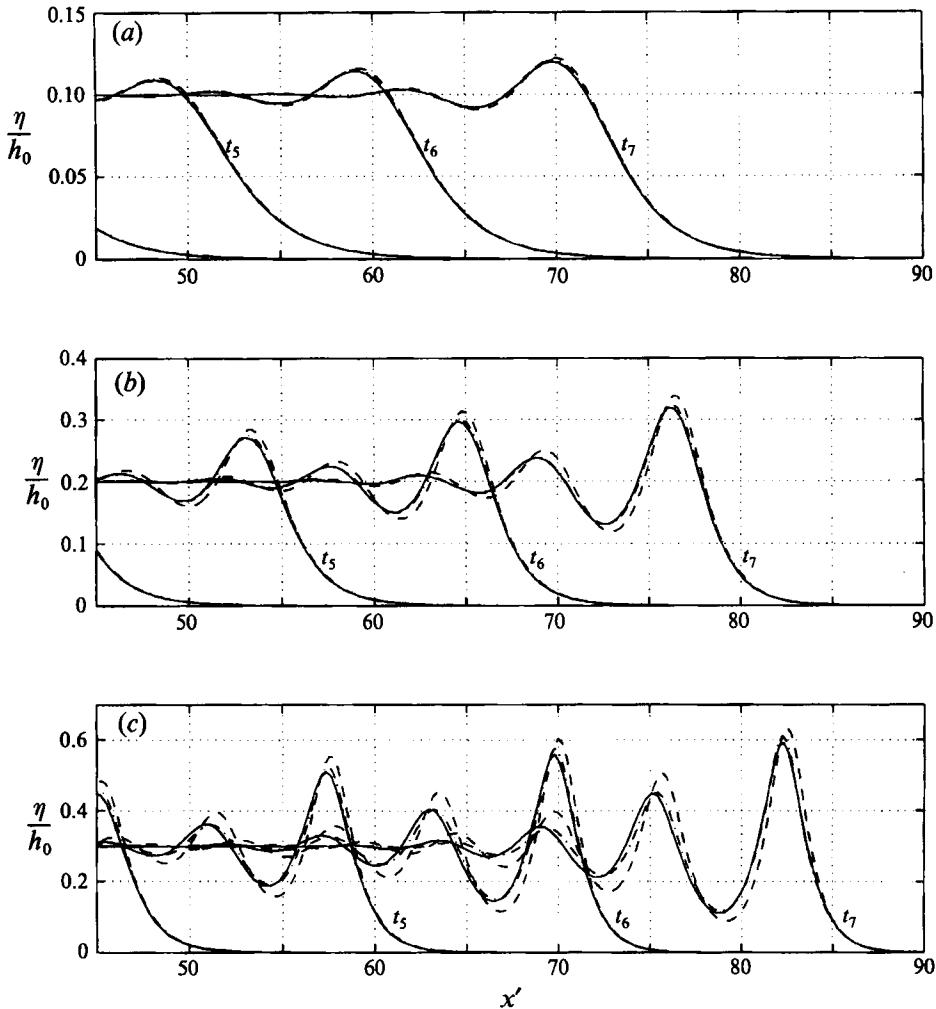
FIGURE 10. Comparison between FNPF (———), BM (- - - - -), and FNBM (— - —) of free surface elevations for undular bores with initial height $\delta = $ (a) 0.10; (b) 0.20; and (c) 0.30, at time t': $t_5 = 50$, $t_6 = 60$, $t_7 = 70$.

6. Conclusions

We have derived a fully nonlinear model for shallow water wave propagation using a standard lowest-order Boussinesq approximation for the fluid kinematics. The internal flow field is defined with respect to the horizontal velocity at a depth z_α in the water column, following the procedure of Nwogu (1993). The resulting equations have improved linear dispersion properties in intermediate depth water and are not limited to small nonlinearity. A high-order numerical model was developed and applied to study two cases of one-dimensional wave propagation. Results from the Boussinesq model with and without the strong nonlinearity extension were compared to results obtained using a BEM solution for fully nonlinear potential flow (FNPF), which served as the reference solution.

From the numerical calculations, we found that in strongly nonlinear situations (such as wave evolution just prior to wave breaking), the FNBM model provides
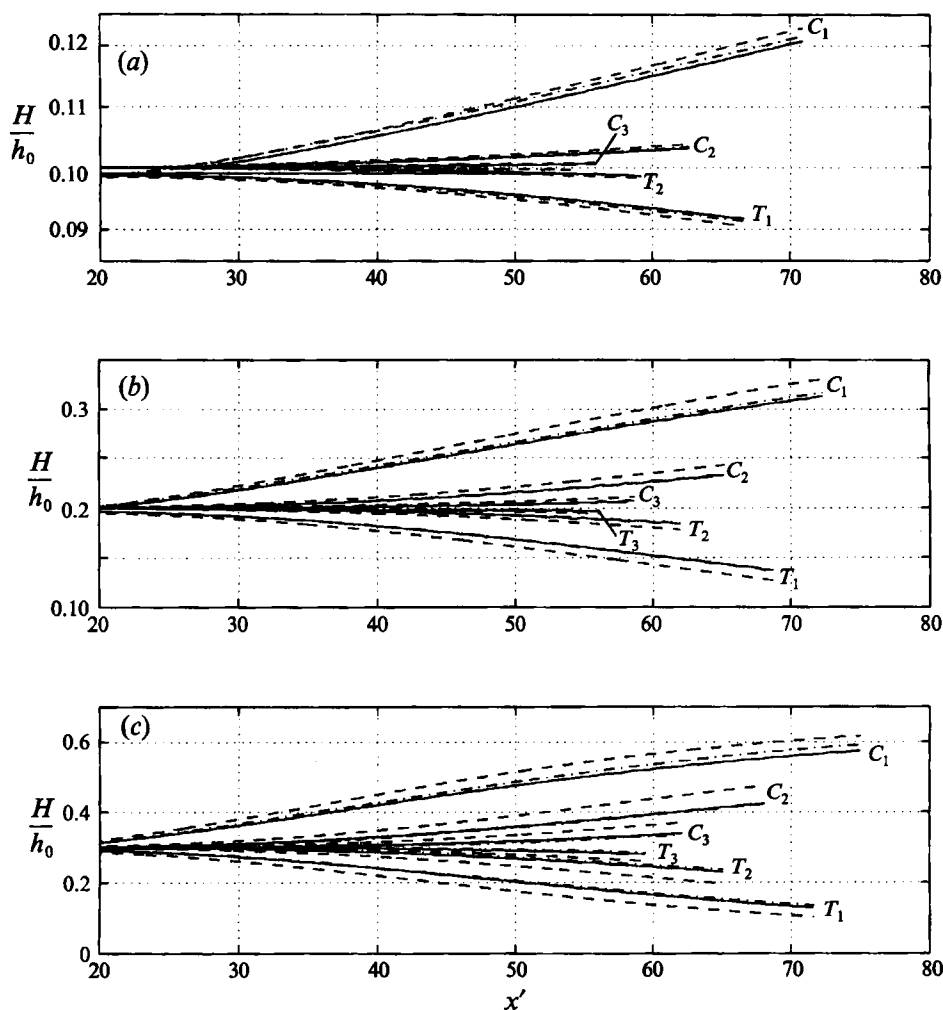
FIGURE 11. Comparison between FNPF (———), BM (- - - - -), and FNBM (— - —) of results for the height of C_1, first; C_2, second; and C_3, third crest and T_1, first; T_2, second; and T_3, third trough, of undular bores with initial height $\delta = (a)$ 0.10; (b) 0.20; and (c) 0.30.

significantly improved predictions of wave heights and internal kinematics relative to the weakly nonlinear BM model. In particular, the magnitudes of horizontal velocities are similar to those predicted by FNPF except at the breaking point, where the FNBM model underpredicts the concavity of the velocity profile. This feature is almost certainly due to the neglect of higher-order terms in the approximation of the velocity potential, and is one indication that an approximation to $O(\mu^4)$, retaining quartic terms in z in the velocity potential, could possibly be profitably pursued. This investigation is presently underway and will be reported on in the near future.

REFERENCES

ABBOTT, M. B., MCCOWAN, A. D. & WARREN, I. R. 1984 Accuracy of short-wave numerical model. *J. Hydr. Engng* **110**, 1287–1301.

CHEN, Y. & LIU, P. L.-F. 1995 Modified Boussinesq equations and associated parabolic models for wave propagation. *J. Fluid Mech.*, in press.

DEMIRBILEK, Z. & WEBSTER, W. C. 1992 Application of the Green-Naghdi theory of fluid sheets to shallow-water wave problems: Report I. Model development. *Tech. Rep.* CERC-92-11. US Army Waterways Experiment Station, Vicksburg, MS.

ELGAR, S. & GUZA, R. T. 1985 Shoaling gravity waves: comparisons between field observations, linear thoery and a nonlinear model. *J. Fluid Mech.* **158**, 47–70.

GORING, D. G. 1978 Tsunamis - the propagation of long waves onto a shelf. PhD dissertation, California Institute of Technology, Pasadena, California.

GREEN, A. E. & NAGHDI, P. M. 1976 A derivation of equations for wave propagation in water of variable depth. *J. Fluid Mech.* **78**, 237–246.

GRILLI, S. T. 1993 Modeling of nonlinear wave motion in shallow water. In *Computational Methods for Free and Moving Boundary Problems in Heat and Fluid Flow* (ed. L.C. Wrobel and C.A. Brebbia), pp. 37–65. Elsevier Applied Sciences, London, UK.

GRILLI, S. T., SKOURUP, J., & SVENDSEN, I. A. 1989 An efficient boundary element method for nonlinear water waves. *Engng Anal. with Boundary Elements* **6**, 97–107.

GRILLI, S. T. & SUBRAMANYA, R. 1994 Numerical modeling of wave breaking induced by fixed or moving boundaries. *J. Comput. Phys.* (submitted).

GRILLI, S. T., SUBRAMANYA, R., SVENDSEN, I. A., & VEERAMONY, J. 1994*a* Shoaling of solitary waves on plane beaches. *J. Waterway Port Coastal & Ocean Engng.* **120**, 609–628.

GRILLI, S. T., SVENDSEN, I. A., & SUBRAMANYA, R. 1994*b* Breaking criterion and characteristics for solitary waves on plane beaches. *J. Waterway Port Coastal & Ocean Engng* (submitted).

KIRBY, J. T. & WEI, G. 1995 A fully nonlinear Boussinesq model for surface waves. II. Bound waves in intermediate water depths. in preparation.

LIU, P. L.-F., YOON, S. B. & KIRBY, J. T. 1985 Nonlinear refraction-diffraction of waves in shallow water. *J. Fluid Mech.* **153**, 184–201.

LONGUET-HIGGINS, M. S. & COKELET, E. D. 1976 The deformation of steep surface waves on water - I. A numerical method of computation. *Proc. R. Soc. Lond.* A**350**, 1–26.

MADSEN, P. A., MURRAY, R. & SØRENSEN, O. R. 1991 A new form of Boussinesq equations with improved linear dispersion characteristics. *Coastal Engng* **15**, 371–388.

MEI, C. C. 1989 *The Applied Dynamics of Ocean Surface Waves.* World Scientific.

MILES, J. & SALMON, R. 1985 Weakly dispersive nonlinear gravity waves. *J. Fluid Mech.* **157**, 519–531.

NWOGU, O. 1993 An alternative form of the Boussinesq equations for nearshore wave propagation. *J. Waterway, Port, Coast. Ocean Engng.* **119**, 618–638.

PEREGRINE, D. H. 1966 Calculations of the development of an undular bores. *J. Fluid Mech.* **25**, 321–330.

PEREGRINE, D. H. 1967 Long waves on a beach. *J. Fluid Mech.* **27**, 815–827.

RYGG, O. B. 1988 Nonlinear refraction-diffraction of surface waves in intermediate and shallow water. *Coastal Engng* **12**, 191–211.

SU, C. H. & GARDNER, C. S. 1969 Korteweg-de Vries equation and generalizations. III. Derivation of the Korteweg-de Vries equation and Burgers equation. *J. Math. Phys.* **10**, 536–539.

TANAKA, M. 1986 The stability of solitary waves. *Phys. Fluids* **29**, 650–655.

WEI, G. AND KIRBY, J. T. 1995 A time-dependent numerical code for extended Boussinesq equations. *J. Waterway Port Coastal Ocean Engng*, in press.

WITTING, J. M. 1984 A unified model for the evolution of nonlinear water waves. *J. Comput. Phys.* **56**, 203–236.

WU, T. Y. T. 1981 Long waves in ocean and coastal waters. *J. Engng Mech.* **107**, 501–522.